Supporting Information

Synergy of Cu-Foam/Sb_2O_3/rGO for Stable Potassium Anodes of High-Rate and Low-Temperature Potassium Metal Batteries

Jing Qi, Chengkai Lin, Shuqi Deng, Yinze Zuo, Hui Zheng, Xuechao Jiao, Wei Yan*, Jiujun Zhang*

Institute for New Energy Materials & Engineering, School of Materials Science & Engineering, Fuzhou University, Fuzhou City, Fujian Province, 350108, P.R. China

Supporting Information

1. Preparation of PTCDA cathode

Firstly, Perylene-3,4,9,10-tetracarboxylic dianhydride (PTCDA) was pretreated and annealed at 420 °C for 2 hours with a heating rate of 5℃/min. The pretreated PTCDA was mixed with Super P and PVDF in the mass ratio of 8:1:1 and then dripped into the appropriate amount of N-methyl-2-pyrrolidone (NMP). After stirring for 6 hours, the slurry was evenly coated on the aluminum foil and dried at 60℃ for 12 hours. The PTCDA mass loading on the cathode was about 1 mg cm^{-2}.

2. Electrochemical measurements

The loss of active K was evaluated using the average coulombic efficiency (CE_{ave}). According to the methods outlined in relevant literature, the average coulombic efficiency of n cycles is determined by the following Equation (S1):

$$CE_{ave}=(nQ_C+Q_S)/(nQ_C+Q_T) \quad (1)$$

where n is the cycled numbers of 10 times, Q_T is 2 mAh cm^{-2} capacity that is initially utilized to deposit K onto the current collector surface, Q_C is a smaller portion of 0.5 mAh cm^{-2}, Q_S is the final stripping capacity after charging to the cut-off voltage of 1 V at the currently density of 0.5 mA cm^{-2}, respectively.

3. Computational Section

Electronic structure calculations were performed with the density functional theory as implemented in the Vienna ab initio simulation package [1, 2], employing the projected augmented wave potential to describe the atomic core electrons and the plane wave basis set to expand the Kohn-Sham electronic states [3]. For the exchange and correlation functional, the generalized gradient approximation (GGA) in the Perdew-Burke-Ernzerhof (PBE) format was used [4]. The kinetic energy cutoff was set to 400 eV and the Gamma centered method was employed for the Brillouin zone sampling for all calculations in this work. For the bulk structures of Cu_2Sb, rGO and Sb_2O_3, the convergence criteria energy for geometric optimization was 10-5 eV/atom and all the atoms were fully relaxed until the atomic forces are less than 0.01 eV $Å^{-1}$. For the other

models, force calculations were set to 0.05 eV $Å^{-1}$ [5].

The Cu_2Sb-K, rGO-K and Sb_2O_3-K model were constructed by the 2×4 supercell. The adsorption energy (E_{ad}) was calculated as: $E_{ad} = (E_{Cu2Sb\text{-}K} - E_{Cu2Sb} - E_K)$, where, $E_{Cu2Sb\text{-}K}$, E_{Cu2Sb} and E_K represent the DFT energies of the K^+ adsorbed Cu_2Sb, the pure Cu_2Sb and the K atom in the bulk phase, respectively.

4. Calculation of rGO and Sb_2O_3 loading on Cu foam

The commercial Cu foam (0.5 mm in thickness) was cut into wafers with a square piece of 20x20 mm，the weight of Cu foam after treated with 3 mol L^{-1} HCl and acetone solution was measured and recorded as m_1, the weight of $Cu@Cu_2Sb$ recorded as m_2, the weight of $Cu@Cu_2Sb@GO$ recorded as m_3 and the weight of $Cu@Sb_2O_3@rGO$ recorded as m_4. The specific weights are shown in Table S1. The mass loading of rGO and Sb_2O_3 were calculated according to those equations by taking Sample 1 as an example:

$$3Cu + Sb^{3+} \rightarrow 3Cu^{+} + Sb \quad (1)$$

$$n_{Sb} = \frac{m_2 - m_1}{M_{sb} - 3 \times M_{Cu}} = \frac{(232.39 - 237.92)\ mg}{(121.8 - 3 \times 63.5)\ mol/g} = 0.08\ mmol \quad (2)$$

$$m_{sb} = n_{Sb} \times 121.8 = 9.8\ mg \quad (3)$$

$$Sb + \frac{3}{4}O_2 \rightarrow \frac{1}{2}Sb_2O_3 \quad (4)$$

$$m_{Sb_2O_3} = n_{Sb} \times \frac{1}{2}M_{Sb_2O_3} = 0.08 \times 145.8 = 11.67\ mg \quad (5)$$

$$\Delta m = n_{Sb} \times (\frac{1}{2}M_{Sb_2O_3} - M_{sb}) = 0.08 \times (\frac{1}{2}291.6 - \frac{3}{4} \times 32 - 121.8) = 1.92\ mg \quad (6)$$

$$m_{rGO} = m_4 - m_2 - \Delta m = 234.72 - 232.39 - 1.92 = 0.41\ mg \quad (7)$$

Therefore, as shown in Table S1, the final mass loading of rGO and Sb_2O_3 on the Cu foam is 0.1~0.11 mg cm^{-2} and 2.92~3.65 mg cm^{-2}, respectively.

Table S1. Table of $Cu@Sb_2O_3@rGO$ mass changes during synthesis.

Mass (mg) / Sample	Cu (m_1)	$Cu@Cu_2Sb$ (m_2)	$Cu@Cu_2Sb@GO$ (m_3)	$Cu@Sb_2O_3@rGO$ (m_4)	Sb_2O_3 (mg cm^{-2})	rGO (mg cm^{-2})

Sample 1	237.92	232.39	232.82	234.72	2.92	0.1
Sample 2	226.21	219.22	219.63	222.00	3.65	0.1
Sample 3	256.39	250.00	250.49	252.61	3.28	0.11

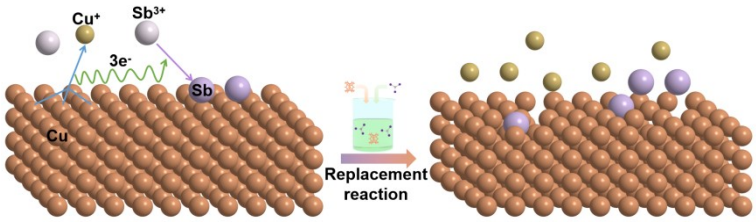

Fig. S1 Schematic illustrating of the replacement reaction.

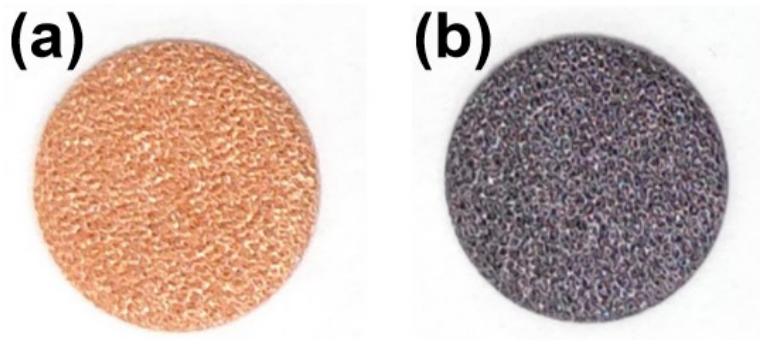

Fig. S2 The digital photos of Cu foam (a) before and (b) after the incubation.

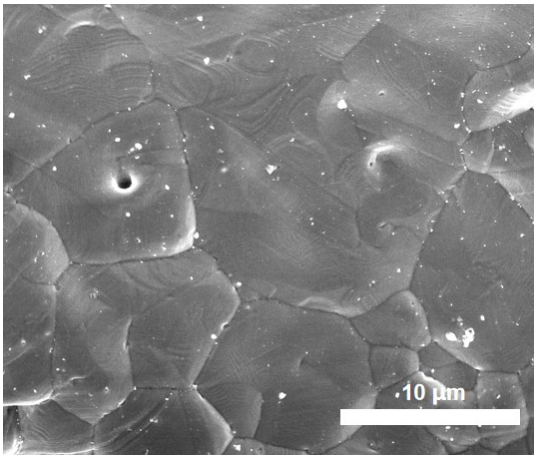

Fig. S3 SEM image of Cu foam.

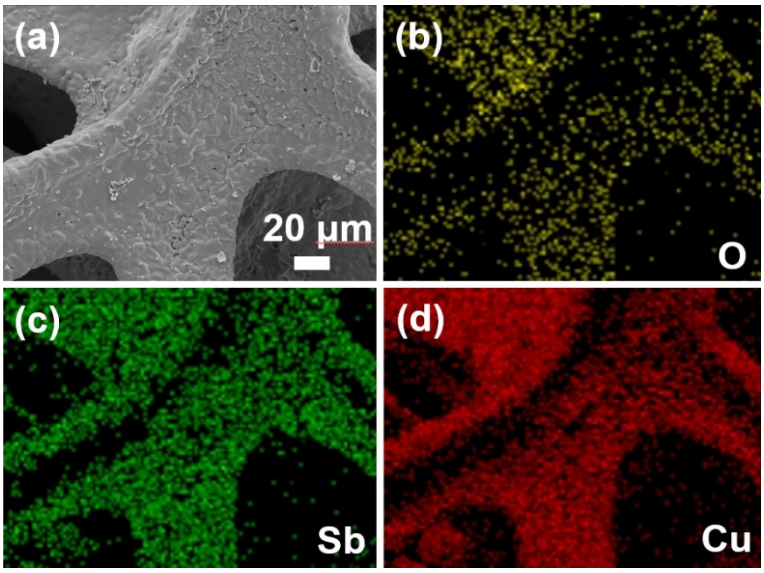

Fig. S4 The EDS of Cu foam after the incubation.

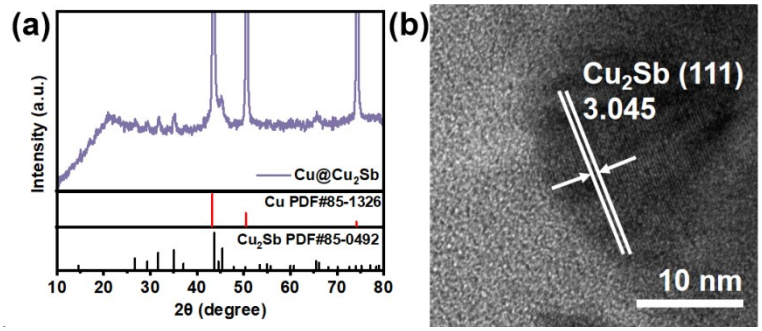

Fig. S5 (a) The XRD patterns of Cu foam and Cu@Cu_2Sb, (b) The HRTEM image of Cu@Cu_2Sb.

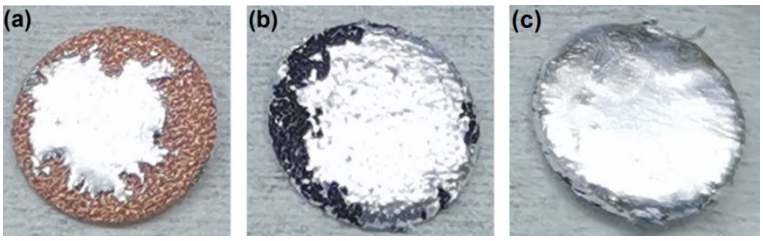

Fig. S6 The digital photos of (a) Cu foam@molten K, (b) Cu@Cu_2Sb@molten K, (c) Cu@Sb_2O_3@rGO@molten K.

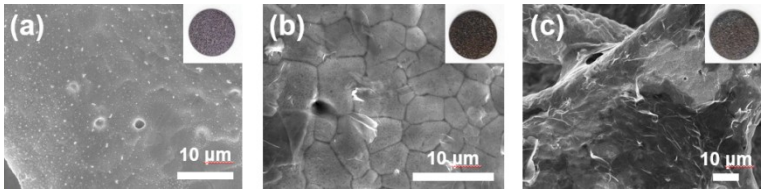

Fig. S7 The SEM images of different current collectors: (a) Cu@Cu_2Sb; (b) GO loaded onto Cu@Cu_2Sb; (c) Cu@Sb_2O_3@rGO.

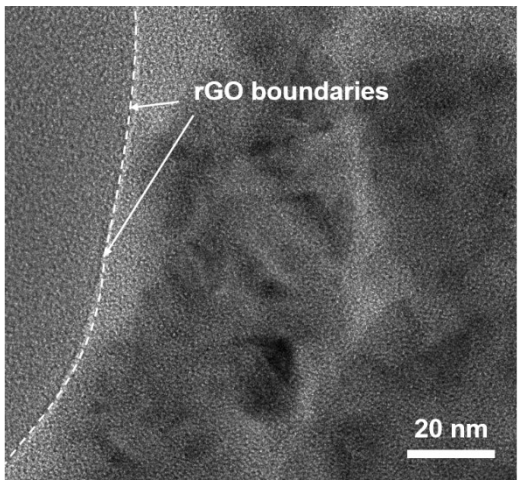

Fig. S8 The TEM image of Cu@Sb_2O_3@rGO.

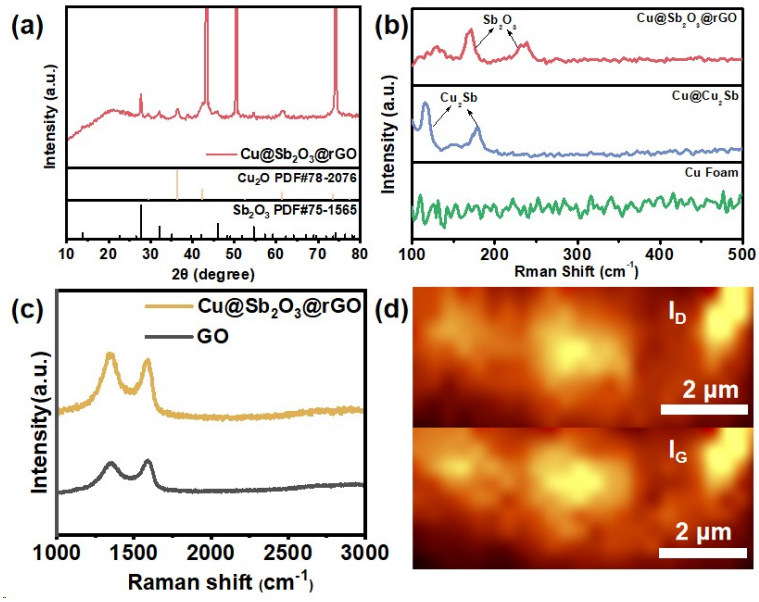

Fig. S9 (a) The XRD pattern of $Cu@Sb_2O_3@rGO$, (b) The Raman spectra of Cu foam, $Cu@Cu_2Sb$ and $Cu@Sb_2O_3@rGO$. (c) the Raman spectra of GO and $Cu@Sb_2O_3@rGO$; (d) the cross-sectional Raman spectroscopic analysis of $Cu@Sb_2O_3@rGO$.

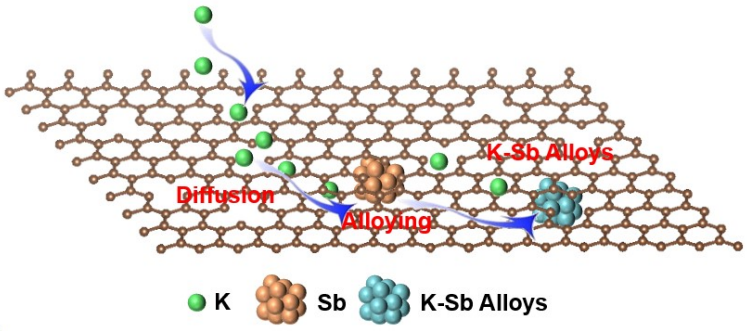

Fig. S10 Illustration of intercalation, diffusion and deposition of K^+ on $Cu@Sb_2O_3@rGO$.

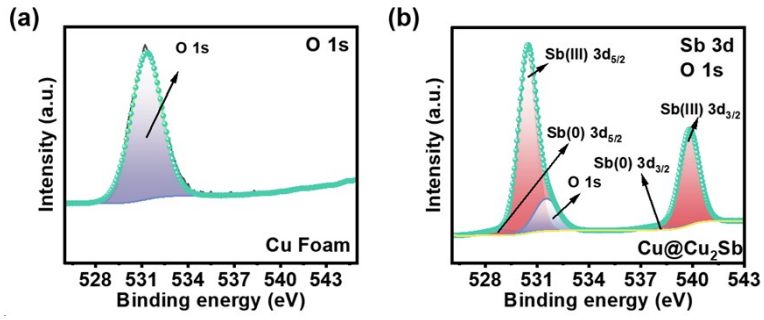

Fig. S11 XPS spectra of O 1s of (a) Cu foam, and (b) O 1s &Sb 3d of Cu@Cu_2Sb.

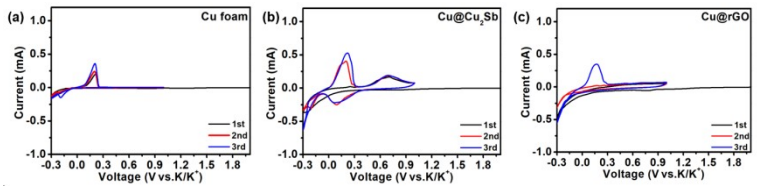

Fig. S12 CV curves of (a) Cu foam, (b) Cu@Cu_2Sb, (c) Cu@rGO.

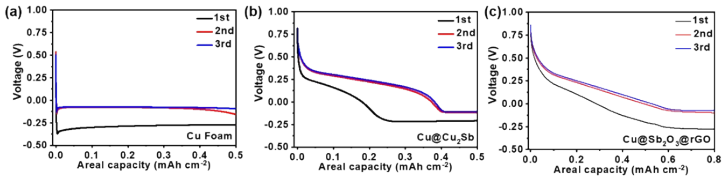

Fig. S13 First three cycles of K plating voltage profile of different current collectors at 0.5 mA cm^{-2} with capacity of 1 mAh cm^{-2}: (a) Cu foam, (b) $Cu@Cu_2Sb$, (c) $Cu@Sb_2O_3@rGO$

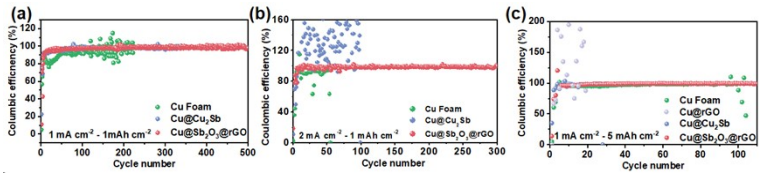

Fig. S14 Coulombic efficiencies (CE) of Cu foam, Cu@Cu_2Sb and Cu@Sb_2O_3@rGO (a) at 1 mA cm^{-2} and 1 mAh cm^{-2}, (b) at 2 mA cm^{-2} and 1 mAh cm^{-2}. (c) Coulombic efficiencies (CE) of Cu foam, Cu@rGO, Cu@Cu_2Sb and Cu@Sb_2O_3@rGO at 1 mA cm^{-2} and 5 mAh cm^{-2}.

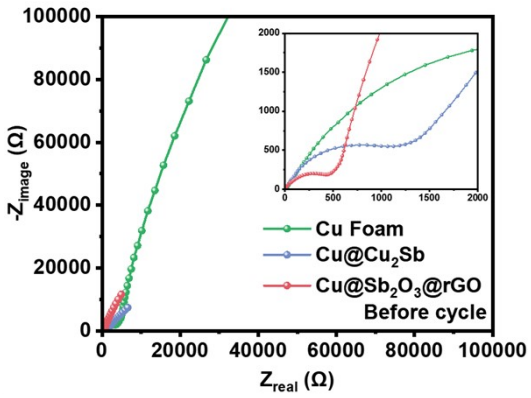

Fig. S15 The Nyquist plots of fresh half cells of different current collectors.

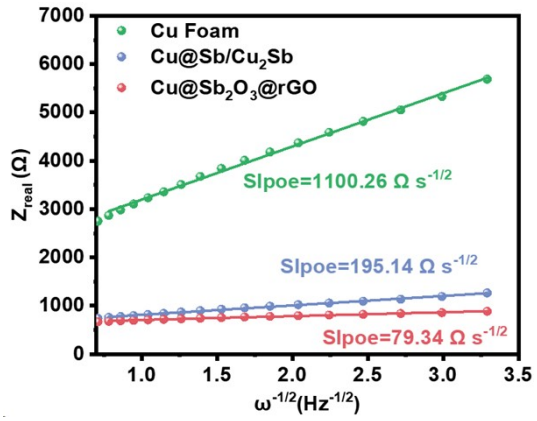

Fig. S16 Extracted |Z| vs. $\omega^{1/2}$ plot in the Warburg region for different current collectors, respectively.

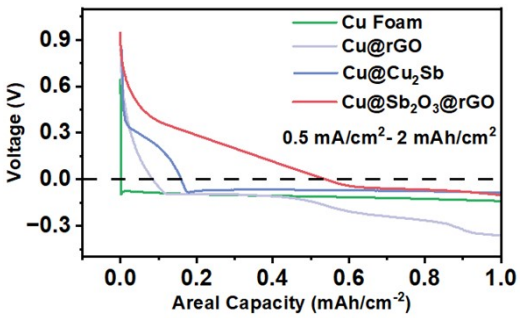

Fig. S17 The third cycle of K plating voltage profile of different current collectors at 0.5 mA cm^{-2} with capacity of 2 mAh cm^{-2}.

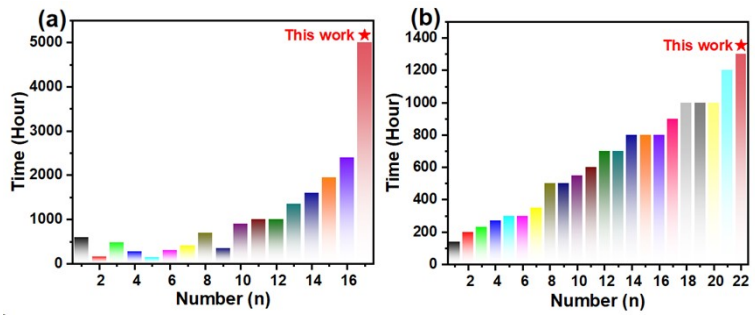

Fig. S18 Comparison of the cycle-life of Cu@Sb_2O_3@rGO with (a) half cells and (b) previously reported symmetric cells that used different strategies to improve the stability of KMBs.

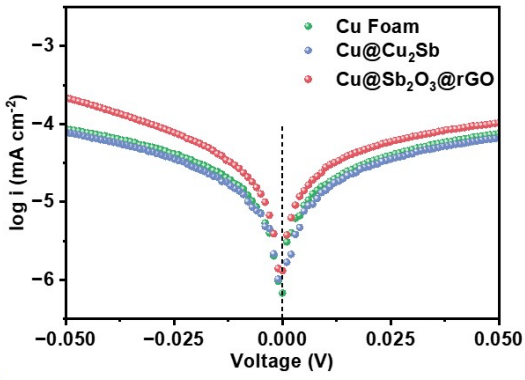

Fig. S19 Tafel curves of Cu Foam@K, Cu@Cu_2Sb@K and Cu@Sb_2O_3 @rGO@K symmetric cells at a scan rate of 0.5 mV s^{-1}.

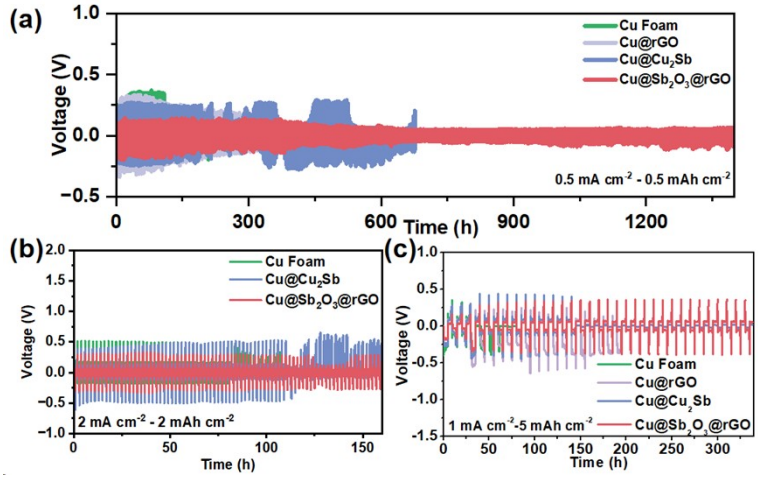

Fig. S20 The cyclic stability of the symmetric cells at (a) 0.5 mA cm^{-2}, 0.5 mAh cm^{-2} (b) 2 mA cm^{-2}, 2 mAh cm^{-2} and (c) 1 mA cm^{-2}, 5 mAh cm^{-2} of different current collectors.

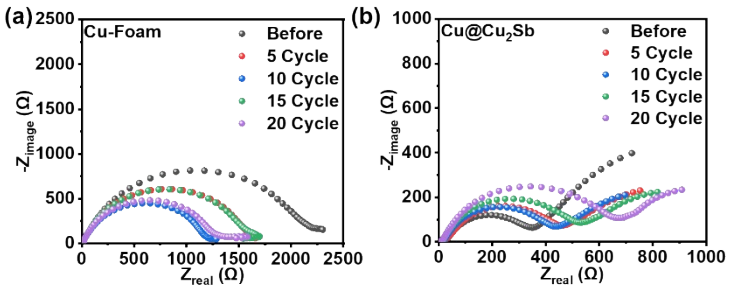

Fig. S21 EIS Nyquist plots of Cu@Cu_2Sb@K||Cu@Cu_2Sb@K and Cu Foam@K||Cu Foam@K symmetric cells collected at 5, 10, 15, 20 cycle.

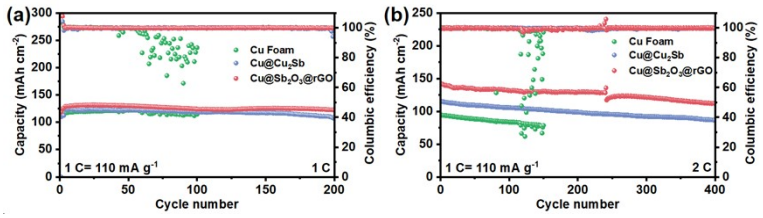

Fig. S22 Cycling at a current rate of (a) 1 C and (b) 2 C of Cu foam@K, Cu@Cu_2Sb@K and Cu@Sb_2O_3@rGO@K full cells (1 C=110 mAh g^{-1}).

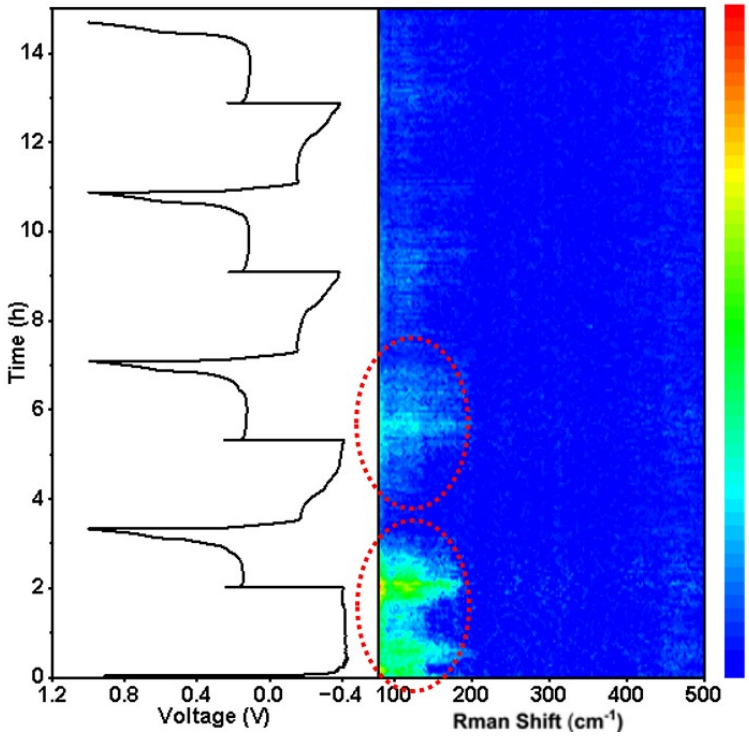

Fig. S23 In-situ Raman spectra of K_xSb near anode electrolyte interface during Cu@Sb_2O_3@rGO operation at the plating/stripping current density of 1 mA cm^{-2} with areal capacity of 2 mAh cm^{-2}.

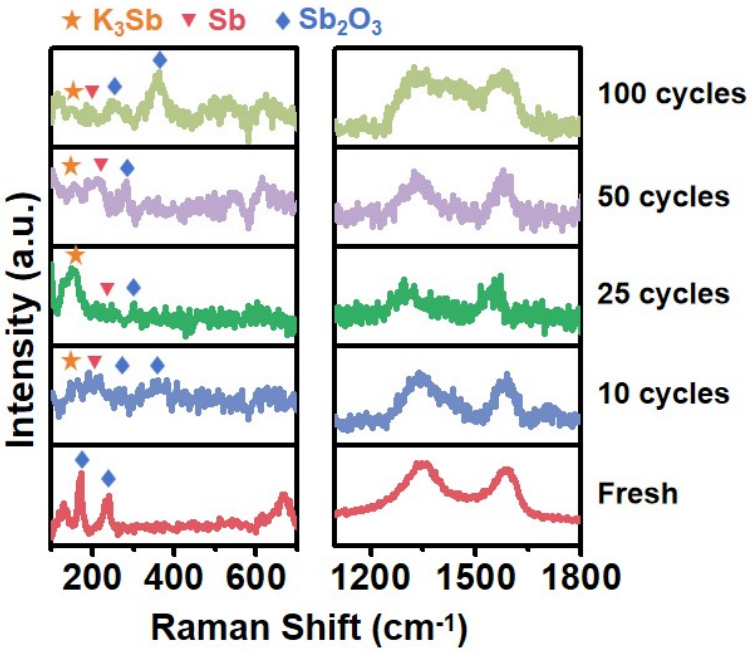

Fig. S24 The Raman spectra of the Cu@Sb_2O_3@rGO with different cycles.

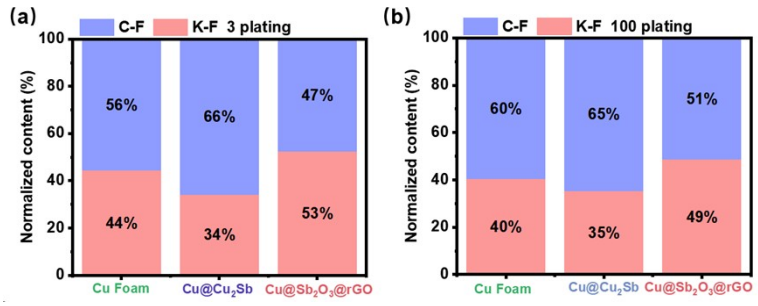

Fig. S25 The corresponding elemental content analysis of F 1s at 3rd and 100th cycle.

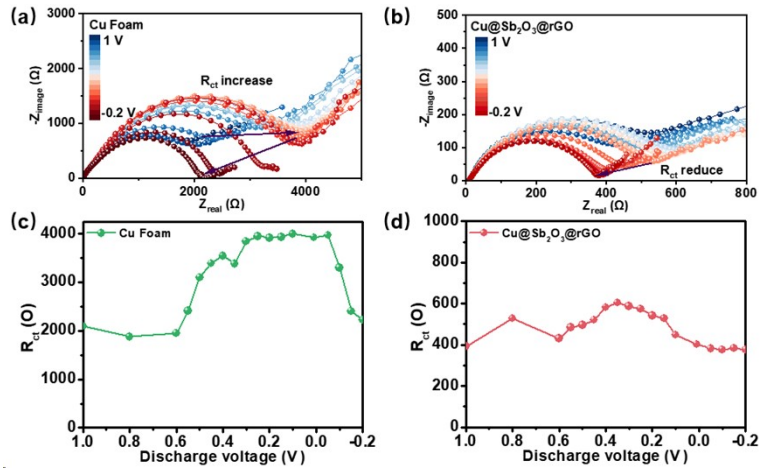

Fig. S26 The EIS Nyquist plots of Cu foam and Cu@Sb_2O_3@rGO electrode were collected at plating current density of 0.5 mA cm^{-2} with different potentials, the voltage range at -0.2 - 1 V.

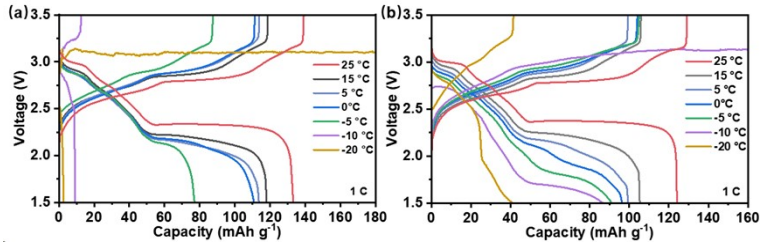

Fig. S27 Charging-discharging profiles of (a) Cu foam@K||PTCDA and (b) Cu@Cu_2Sb@K||PTCDA full cell at 1 C for different temperatures.

Table S2. Half cell comparison.

Materials	Electrolytes	Current-Capacity (mA cm^{-2} - mAh cm^{-2})	Cycle numbers	CE	Reference
Bare Cu foil	1M or 5M KFSI in DME	0.05-0.15	100	99%	6
rGO@3D-Cu	0.8 M KPF_6 in EC/DEC/PC	0.5-0.5	100 (160h)	76%	7
DN-MXene/CNT	0.8 M KPF_6 in EC/DEC	0.5-1	120	93.1%	8
Cu_3Pt-Cu mesh	1 M KFSI in DME	0.5-0.5	150 (270h)	95%	9
Ag-CC	0.8 M KPF_6 in EC/DEC	1-0.5	150	99.5%	10
PCNF@SnO_2-K	1 M KFSI in DME	1-1	150	98.3%	11
AlF_3@PP	4 M KFSI inDME	0.5-0.5	200 (398h)	-	12
CBC-K	1 M KFSI in DME	1-1	350	~98%	13
CoZn@HCT	1 M KFSI in DME	1-0.5	350	96.9%	14
Pd/Cu foam	3 M KFSI in DME	0.5-0.5	450	98%	15
Al@G	4 M KFSI in DME	0.5-0.5	500	99%	16
Cu@SKS	4 M KFSI in DME	1-1	500 (1000h)	99.1%	17
Bi_{80}/NrGO	3 M KFSI in DME	0.1-0.1	675 (1350h)	99.6%	18
NC@GDY-Al	4 M KFSI in DME	0.2-0.2	800	99.93%	19
Al@Al	4 M KFSI in DME	0.5-0.5	1000 (1950h)	98.9%	20
Cu@Sb_2O_3@rGO	3M KFSI in DME	0.5-1	600 (2400h)	99.9&	This Work
		0.5-2	620 (~5000h)	99.9%	

Table S3. Symmetric cell comparison.

Materials	Current density (mA cm^{-2})	Cycling stability (hour)	Reference
CFC/KOL@Na-K	0.4	140	21
rGO@3D-Cu	0.5	200	7
K-ACM	1	230	22
rGO-K	2	270	23
K@Cu_3Pt-Cu	0.5	300	9
K@DN-Mxene/CNT	0.5	300	8
Amine-Wetting K@CC	1	350	24
Sn@3D-K	0.2	500	25
K@CNTs	1	500	26
KxPy@K	0.5	550	27
Na-K@rGO	1	600	28
PVA-Borax@Cu	0.5	700	29
K@Ag-CC	0.5	700	10
K@K_2Te	0.5	800	30
K@SnS_2@CP	0.25	800	31
K-OPCMs/K	1	800	32
Cu@SKS	1	900	17
AgLF/NNFS-NaK	0.4	1000	33
K@hoCNT	0.5	1000	34
K_2Se/Cu@K	0.5	1000	35
CoZn@HCT@K	0.5	1200	14
Cu@Sb_2O_3@rGO	0.2	1300	This Work

Table S4. The I_D/I_G values of the Cu@Sb_2O_3@rGO with different cycles.

Sample	Fresh	10 cycles	25 cycles	50 cycles	100 cycles
I_D/I_G	1.03	1.04	1.03	1.03	1.04

References

1. J. P. Perdew, J. A. Chevary, S. H. Vosko, K. A. Jackson, M. R. Pederson, D. J. Singh and C. Fiolhais, *Phys. Rev. B*, 1992, **46**, 6671-6687.

2. G. Kresse and J. Furthmuller, *Phys. Rev. B*, 1996, **54**, 11169-11186.

3. P. E. Blöchl, *Phys. Rev. B*, 1994, **50**, 17953-17979.

4. J. P. Perdew, K. Burke and M. Ernzerhof, *Phys. Rev. Lett.*, 1996, **77**, 3865-3868.

5. R. F. W. Bader, *Phys. Rev. B*, 1994, **49**, 13348-13356.

6. N. Xiao, W. D. McCulloch and Y. Y. Wu, *J. Am. Chem. Soc.*, 2017, **139**, 9475-9478.

7. P. Liu, Y. Wang, Q. Gu, J. Nanda, J. Watt and D. Mitlin, *Adv. Mater.*, 2019, **32**, e1906735.

8. X. Tang, D. Zhou, P. Li, X. Guo, B. Sun, H. Liu, K. Yan, Y. Gogotsi and G. Wang, *Adv. Mater.*, 2019, **32**, e1906739.

9. J. Wang, J. Yuan, C. Chen, L. Wang, Z. Zhai, Q. Fu, Y. Liu, L. Dong, W. Yan, A. Li and J. Zhang, *Nano Energy*, 2020, **75**, 104914.

10. J. H. Zhang, Y. Q. Li, L. P. Zhu, X. L. Wang and J. P. Tu, *Chem. Eng. J.*, 2022, **449**, 137659.

11. X. X. Zhao, F. J. Chen, J. Q. Liu, M. R. Cheng, H. Su, J. B. Liu and Y. H. Xu, *J. Mater. Chem. A*, 2020, **8**, 5671-5678.

12. P. Liu, H. Hao, H. Celio, J. Cui, M. Ren, Y. Wang, H. Dong, A. R. Chowdhury, T. Hutter, F. A. Perras, J. Nanda, J. Watt and D. Mitlin, *Adv. Mater.*, 2021, **34**, e2105855.

13. M. F. Zhou, W. Y. Qi, Z. M. Hu, M. R. Cheng, X. X. Zhao, P. X. Xiong, H. Su, M. J. Li, J. M. Hu and Y. H. Xu, *ACS Appl. Mater. Interfaces*, 2021, **13**, 17629-17638.

14. G. Z. Cheng, S. Liu, X. J. Wang, X. R. Li, Q. D. Y. X. Su, J. Shi, M. H. Huang, Z. C. Shi, H. L. Wang and Z. H. Yan, *ACS Appl. Mater. Interfaces*, 2022, **14**, 45364-45372.

15. J. Y. Wang, W. Yan and J. J. Zhang, *Nano Energy*, 2022, **96**, 107131.

16. Y. Zhao, B. Z. Liu, Y. Y. Yi, X. Y. Lian, M. L. Wang, S. Li, X. Z. Yang and J. Y. Sun, *Adv. Mater.*, 2022, **34**, e2202902.

17. J. Xie, Y. Ji, L. Ma, Z. Wen, J. Pu, L. Wang, S. Ding, Z. Shen, Y. Liu, J. Li, W. Mai and G. Hong, *ACS Nano*, 2023, **17**, 1511-1521.

18. Y. H. Feng, A. M. Rao, J. Zhou and B. A. Lu, *Adv. Mater.*, 2023, **35**, e2300886.

19. Y. Y. Yi, J. Q. Li, Z. X. Gao, W. F. Liu, Y. Zhao, M. L. Wang, W. Zhao, Y. Han, J. Y. Sun and J. Zhang, *Adv. Mater.*, 2022, **34**, e2202685.

20. P. C. Liu, Y. X. Wang, H. C. Hao, S. Basu, X. Y. Feng, Y. X. Xu, J. A. Boscoboinik, J. Nanda, J. Watt and D. Mitlin, *Adv. Mater.*, 2020, **32**, e2002908.

21. L. Y. Zhang, X. H. Xia, Y. Zhong, D. Xie, S. F. Liu, X. L. Wang and J. P. Tu, *Adv. Mater.*, 2018, **30**, e1804011.

22. L. Qin, Y. Lei, H. W. Wang, J. H. Dong, Y. Y. Wu, D. Y. Zhai, F. Y. Kang, Y. Tao and Q. H. Yang, *Adv. Energy Mater.*, 2019, **9**, 1901427.

23. Z. H. Wei, A. X. Wang, X. Z. Guan, G. J. Li, Z. W. Yang, C. D. Huang, J. Zhang, L. B. Ren, J. Y. Luo and X. J. Liu, *Energy Environ. Mater.*, 2022, **5**, 1278-1284.

24. J. S. Meng, H. Z. Zhu, Z. T. Xiao, X. C. Zhang, C. J. Niu, Y. K. Liu, G. P. Jiang, X. P. Wang, F. Qiao, X. F. Hong, F. Liu, Q. Q. Pang and L. Q. Mai, *Acs Nano*, 2022, **16**, 7291-7300.

25. M. Ye, J. Y. Hwang and Y. K. Sun, *ACS Nano*, 2019, **13**, 9306-9314.

26. Y. J. Yang, C. Huang, Y. Zhang, Y. X. Wu, X. Zhao, Y. Qian, G. Chang, Q. L. Tang, A. P. Hu and X. H. Chen, *ACS Appl. Mater. Interfaces*, 2022, **14**, 55577-55586.

27. P. C. Shi, S. P. Zhang, G. X. Lu, L. F. Wang, Y. Jiang, F. F. Liu, Y. Yao, H. Yang, M. Z. Ma, S. F. Ye, X. Y. Tao, Y. Z. Feng, X. J. Wu, X. H. Rui and Y. Yu, *Adv. Energy Mater.*, 2021, **11**, 2003381.

28. T. T. Luo, Q. Q. Zhao, Y. W. Liu, W. D. Meng, Q. Sun, L. Dai, S. Liu and L. Wang, *Ecomat*, 2022, **4**, e12203.

29. S. Wang, Y. Yan, D. Xiong, G. Li, Y. Wang, F. Chen, S. Chen, B. Tian and Y. Shi, *Angew. Chem. Int. Ed.*, 2021, **60**, 25122-25127.

30. H. Yang, F. He, M. Li, F. Huang, Z. Chen, P. Shi, F. Liu, Y. Jiang, L. He, M. Gu and Y. Yu, *Adv. Mater.*, 2021, **33**, e2106353.

31. M. Han, J. Jiang, S. Lu, Y. Jiang, W. Ma, X. Liu, B. Zhao and J. Zhang, *ACS Appl.*

Mater. Interfaces, 2022, **14**, 900-909.

32. S. H. Xie, W. Xie, Q. F. Zhang, X. L. Cheng, X. P. Ouyang and B. A. Lu, *Adv. Funct. Mater.*, 2023, **33**, 2302880.

33. Y. S. Luo, P. Z. Mou, W. L. Yuan, L. P. Li, Y. Z. Fan, Y. Chen, X. M. Chen, J. Shu and L. Y. Zhang, *Chem. Eng. J.*, 2023, **452**, 139157.

34. Y. Liu, Y. Shi, C. Gao, Z. Shi, H. Ding, Y. Feng, Y. He, J. Sha, J. Zhou and B. Lu, *Angew. Chem. Int. Ed.*, 2023, e202300016.

35. F. F. Liu, L. F. Wang, F. X. Ling, X. F. Zhou, Y. Jiang, Y. Yao, H. Yang, Y. Shao, X. J. Wu, X. H. Rui, C. X. He and Y. Yu, *Adv. Funct. Mater.*, 2022, **32**, 2210166.